Turbulent transport efficiency and the ejection-sweep motion for momentum and heat on sloping terrain covered with vineyards

UNIVERSITÀ DEGLI STUDI DI TORINO

Agricultural and Forest Meteorology, vol. 162-163, (2012),

DOI:10.1016/j.agrformet.2012.04.012

Turbulent transport efficiency and the ejection-sweep motion for momentum and heat on sloping terrain covered with vineyards

(MANUSCRIPT)

Caterina Francone[1,2,3,*], Gabriel G. Katul[4,5,6], Claudio Cassardo[3,7] and Renzo Richiardone[3,7]

[1]Department of Plant Production, CASSANDRA, University of Milan, via Celoria 2, 20133 Milano, Italy.

[2]Departiment of Physics, University of Turin, Via Pietro Giuria 1, 10125 Torino, Italy.

[3]Department of Mechanical and Aerospace Engineering, Polytechnic of Turin, Corso Duca degli Abruzzi 24, 10129 Torino, Italy.

[4]Nicholas School of the Environment, Box 90328, Duke University, Durham, North Carolina, U.S.A.

[5]Department of Civil and Environmental Engineering, Duke University, Durham, North Carolina, U.S.A.

[6]Department of Environment, Land and Infrastructure Engineering, Polytechnic of Turin, Corso Duca degli Abruzzi 24, 10129 Torino, Italy.

[7] CINFAI, National Inter/University Consortium for Physics of the Atmosphere and Hydrosphere, Italy.

* Corresponding Author, Tel. +39 02 50316578, E-mail: caterina.francone@unimi.it, Fax: +39 02 50316575

Abstract

In boundary layer flows, it is now recognized that the net momentum and mass exchange rates are dominated by the statistical properties of ejecting and sweeping motion often linked to the presence of coherent turbulent structures. Over vineyards, three main factors impact the transport properties of such coherent motion: presence of sloping terrain, variations in leaf area index (LAI) during the growing season, and thermal stratification. The effect of these factors on momentum and heat transport is explored for three vineyard sites situated on different slopes. All three sites experience similar seasonal variation in LAI and mean wind conditions. The analysis is carried out using a conventional quadrant analysis technique and is tested against two models approximating the joint probability density function (JPDF) of the flow variables. It is demonstrated that a Gaussian JPDF explains much of the updraft and downdraft statistical contributions to heat and momentum transport efficiencies for all three sites. An incomplete or truncated third-order cumulant expansion method (ICEM) of the JPDF that retains only the mixed moments and ignores the skewness contributions describes well all the key properties of ejections and sweeps for all slopes, LAI, and stability classes. The implication of these findings for diagnosing potential failures of gradient-diffusion theory over complex terrain is discussed. Because only lower order moments are needed to describe the main characteristics of the JPDF, the use of the Moving Equilibrium Hypothesis (MEH) to predict these moments from the locally measured sensible heat flux and friction velocity is explored. Provided the planar fit coordinate transformation is applied to the data, the MEH can describe these statistical moments at all three sites regardless of terrain slopes and LAI values.

Keywords: coherent motion; cumulant expansions; heat and momentum transfer; sloping terrain; vineyards.

1. Introduction

Drag alterations, wind sheltering, and other bulk flow properties over vineyards have been studied over the past three decades with a 'lens' on how shifts in mean wind direction paralleling or orthogonal to vine rows impact them (e.g. Hicks, 1973; Weiss and Allen, 1976; Riou et al., 1987). However, more complex turbulent features such as ejections and sweeps characterizing non-local large-scale motion and responsible for a significant component of the momentum and heat transport has received disproportionately less attention.

The relative importance of ejections and sweeps on momentum and heat transport, conventionally attributed to the presence of ‘coherent motion’, has been extensively studied in turbulent boundary layers over flat surfaces (Kline et al., 1967; Robinson, 1991) and over canopies (Raupach and Thom, 1981; Shaw et al., 1983; Gao et al., 1989; Raupach et al., 1996; Katul et al., 1997a; Finnigan, 2000). Detecting signatures of coherent motion in velocity and scalar concentration time series and deriving quantitative conclusions about their mass and momentum transport properties proliferated following conditional sampling techniques and quadrant analysis (see Lu and Willmarth, 1973; Antonia, 1981; Cantwell, 1981 for reviews). However, linkages between the statistical properties of ejections/sweeps and updrafts/downdrafts, as derived from the latter techniques and classical turbulence closure modeling, has resisted complete theoretical treatment.

Progress in this area has benefited by verified relations between these statistical properties and the parameters describing the joint probability density function (JPDF) of turbulent flow variables. One example is the seminal work of Nakagawa and Nezu (1977), and later Raupach (1981), who employed a two-dimensional Gram-Charlier *cumulant expansion method* (CEM) to analytically couple the imbalance in turbulent stress contribution of sweeps and ejections to turbulent diffusion processes through the third (or mixed) moments. Linking the statistical properties of ejecting and sweeping motion to the triple moments illustrates how classical gradient-diffusion schemes for

momentum and heat, now widely used in describing flow over complex terrain (e.g. Raupach et al., 1992; Raupach and Finnigan, 1997; Wilson et al., 1998; Finnigan and Belcher, 2004; Katul et al., 2006; Poggi et al., 2008), becomes perturbed by the strength of these motions. In particular, flume experiments (Poggi et al., 2004) and studies on flows inside dense canopies (Cava et al., 2006) already reported how gradient-diffusion schemes become modified by ejecting and sweeping motion via a CEM approach, while a theoretical framework that bridges these studies to failure of gradient-diffusion theories (beyond qualitative arguments) is currently lacking. An additional linkage between the flow property describing the transport efficiency of updrafts and downdrafts and its prediction from a Gaussian JPDF, surprisingly with no adjustments for the effects of third moments, was employed by Wyngaard and Moeng (1992) in their Large Eddy Simulation studies and by Bou-Zeid and Li (2011) in experiments over lakes and vineyards situated on a flat terrain.

Flow over vineyards is generally complicated by numerous processes typically absent from classical boundary-layer studies. Vineyards, for example, are often situated on sloping terrain, are characterized by large changes in LAI during the growing season, and are immersed in a stratified boundary layer. Because of these natural complications, the primary goals here are to explore how sloping terrain, varying LAI, and thermal stratification jointly impact the updraft/downdraft and ejection/sweep properties of momentum and heat transfer and their links to lower-order moments. Lastly, the employment of a variant on the so-called 'Moving Equilibrium Hypothesis' (hereafter referred to as MEH; after Kader and Yaglom, 1978), permitting the estimation of these lower order moments from local flux parameters, is tested. Whether the ICEM can provide links between ejections and sweeps and lower-order moments (predicted by MEH) for flow over complex terrain experiencing large fluctuations in thermal stratification and LAI is considered. This generalization of ICEM has not been previously attempted and constitutes one of the main novelty of the study here. Moreover, practical problems such as quantifying the effects heat accumulation for sunward facing slopes, preventing inversion layers from forming at near-freezing conditions, and

transporting dryer air from aloft thereby enhancing the role of fungicides in controlling fungal diseases can benefit from this study. As proposed here, future modeling may adjust for biases to gradient-diffusion theory introduced by an imbalance between ejections and sweeps, provided the sign of this imbalance is known.

The study objectives are addressed by analyzing time series of velocity and air temperature sampled at 21 Hz above three vineyard sites (*Vitis vinifera* L., Barbera variety) situated in the Monferrato and Langhe sub-regions of the Piemonte region of Northern Italy. These three sites are characterized by slopes ranging from mild to steep. The experiment duration covered an entire season in which LAI varied from 1.0 $m^2\ m^{-2}$ to 3.5 $m^2\ m^{-2}$ at all three sites.

2. Theory

2.1. Nomenclature

For an arbitrary flow variable *s*, $\overline{s}$ is defined as the time average over a 30-minute interval, and s' is defined as the instantaneous turbulent excursion from this time-averaged quantity, such that $\overline{s'} = 0$. The terms 'ejections', 'sweeps', 'direct flux', 'indirect flux', 'updrafts', and 'downdrafts' are defined here via quadrant analysis as reviewed elsewhere (e.g., Antonia, 1981). Quadrant analysis refers to the joint scatter across four quadrants defined by a Cartesian plane whose abscissa is an arbitrary flow variable s' (e.g., $s' = u', T'$) and whose ordinate is generally the vertical velocity w'. For flow variables where usually $\overline{w's'} < 0$, such as momentum ($s' = u'$), the four quadrants indicate four possible modes of momentum transfer: events in quadrants II ($u' < 0,\ w' > 0$) and IV ($u' > 0$ and $w' < 0$) are conventionally labeled as ejections and sweeps respectively, while events in quadrants I ($u' > 0$ and $w' > 0$) and III ($u' < 0$ and $w' < 0$) are called outward and inward interactions, respectively. Events contributing to $u'w' < 0$ (i.e. quadrants II and IV) are labeled as 'direct' fluxes while events contributing to $u'w' > 0$ (quadrants I and III) are labeled as 'indirect' or

'back' fluxes. Opposite quadrants define fluxes for variables where $\overline{w's'} > 0$, as is common for daytime air temperature ($s' = T'$).

2.2 Direct fluxes, back fluxes, and transport efficiency

The transport efficiency e_t is defined as

$$e_t = \left| \frac{F_{Direct} - F_{Back}}{F_{Direct}} \right| \tag{1}$$

where F_{Direct} and F_{Back} are the direct and back (or indirect) fluxes integrated over the 30 minute time-averaging interval, respectively. For momentum transfer, F_{Direct} is the accumulation of all events within the 30-minute averaging period situated in quadrants II and IV, while F_{Back} is the accumulation of all events situated in quadrants I and III. The same definitions for F_{Direct} and F_{Back} hold for heat transport when $\overline{w'T'} < 0$, while the quadrants associated with F_{Direct} and F_{Back} are reversed when $\overline{w'T'} > 0$. For a Gaussian JPDF, it can be shown that (Wyngaard and Moeng, 1992)

$$e_t = \frac{2\pi |R_{ws}|}{2\sqrt{1 - R_{ws}^2} + \pi |R_{ws}| + 2|R_{ws}| \sin^{-1}(|R_{ws}|)} \tag{2}$$

where R_{ws} is the correlation coefficient between w' and s'.

2.3 Ejections and sweeps contribution to momentum and heat fluxes

Nakagawa and Nezu (1977) and Raupach (1981) defined the imbalance in the contributions of sweeps and ejections to momentum transfer using the difference in stress fraction contributions of quadrant IV and quadrant II as:

$$\Delta S_o = \frac{\overline{u'w'}_{IV} - \overline{u'w'}_{II}}{\overline{u'w'}} \tag{3}$$

where $\overline{u'w'}$ is the total momentum flux and $\frac{\overline{u'w'}_{IV}}{\overline{u'w'}}$ and $\frac{\overline{u'w'}_{II}}{\overline{u'w'}}$ are the stress fractions in quadrant IV and II, respectively. This definition ensures that ΔS_o is bounded between –1 and 1 (assuming $\left|\overline{u'w'}\right| > 0$). Based on this definition, sweeps (ejections) dominate the momentum transfer when $\Delta S_o > 0$ ($\Delta S_o < 0$). Because ΔS_o becomes ill defined when $\left|\overline{u'w'}\right| \to 0$, purely convective and very stable thermal stratification regimes cannot be treated in this work.

Using the Gram-Charlier series expansion of the JPDF (Kampé de Fèriet, 1966) truncated to the third order (i.e., CEM), Raupach (1981) demonstrated that:

$$\Delta S_o = \frac{1+R_{uw}}{R_{uw}\sqrt{2\pi}}\left[\frac{2C_1}{(1+R_{uw})^2}+\frac{C_2}{1+R_{uw}}\right] \tag{4}$$

where,

$$\begin{aligned} C_1 &= (1+R_{uw})\left[\frac{1}{6}(M_{03}-M_{30})+\frac{1}{2}(M_{21}-M_{12})\right] \\ C_2 &= -\left[\frac{1}{6}(2-R_{uw})(M_{03}-M_{30})+\frac{1}{2}(M_{21}-M_{12})\right] \end{aligned} \tag{5}$$

and $R_{uw}=\frac{\overline{u'w'}}{\sigma_u\sigma_w}$, $M_{\alpha\beta}=\frac{\overline{u'^{\alpha}w'^{\beta}}}{\sigma_u^{\alpha}\sigma_w^{\beta}}$, $\sigma_s=\sqrt{\overline{s'^2}}$ and where $u'^{\beta}\big|_{\beta=2} \to u'^2$, etc... and repeated indices do not imply summation.

Katul et al. (1997a,b) noted that, for the range of skewness values encountered in the atmospheric boundary layer, the contribution from $\frac{1}{6}(M_{03}-M_{30})$ is small relative to $\frac{1}{2}(M_{21}-M_{12})$. This assumption allows further simplification to equation (4) resulting in:

$$\Delta S_o \approx \frac{1}{2R_{uw}\sqrt{2\pi}}(M_{21}-M_{12}) \tag{6}$$

where

$$M_{21} = \frac{\overline{u'u'w'}}{\sigma_u^2 \sigma_w}$$
$$M_{12} = \frac{\overline{u'w'w'}}{\sigma_u \sigma_w^2} \qquad (7)$$

Equation 6 is hereafter referred to as an incomplete cumulant expansion (ICEM) because of the elimination of the two velocity skewnesses in the third-order cumulant expansion of the JPDF.

For heat transport with $\overline{w'T'} < 0$, the derivation and nomenclature remains the same as for momentum. However, when $\overline{w'T'} > 0$, the imbalance in the contribution of sweeps and ejection is evaluated by using the difference in heat flux fraction originating from quadrants III and I. Moreover, the application of the CEM and ICEM formulations requires a minor coordinate transformation as discussed elsewhere (Katul et al., 1997a,b). Finally, it should be noted that when JPDF is Gaussian (as assumed in the analysis of e_t), $\Delta S_o = 0$. Stated differently, the asymmetry in the JPDF is necessary for sweeps and ejections to contribute differently to turbulent fluxes. The fact that $\Delta S_o \neq 0$ and may vary with z has important implications to gradient-diffusion closure models. To illustrate, consider the sensible heat flux obtained from the heat budget equation for a planar, homogeneous, stationary, and high Reynolds number flow (Garratt, 1992):

$$\overline{w'T'} = \frac{\tau}{C_T}\left(-\sigma_w^2 \frac{d\overline{T}}{dz} - \frac{d\overline{T'w'w'}}{dz} + \frac{4}{3}\frac{g}{\overline{T}}\sigma_T^2 \right) \qquad (8)$$

where, τ is a relaxation time scale, C_T is a closure constant, g is the gravitational acceleration, and $\sigma_T^2 = \overline{T'T'}$. It is clear from this expression that for near-neutral conditions (last term on the right-hand side of Eqn. 8 can be neglected) and in the absence of any flux transport term, gradient diffusion theory often used in modeling flow over vegetation in complex terrain is recovered with a turbulent diffusivity given by $\tau\sigma_w^{\,2}/C_T$. Using the ICEM and assuming a linear relationship between M_{12} and M_{21} as shown in wind tunnel experiments and for dense canopy (Raupach, 1981;

Cava et al., 2006), the flux-transport term responsible for perturbing gradient-diffusion theory can now be linked to ejections and sweeps via

$$M_{12} = \frac{\overline{T'w'w'}}{\sigma_T \sigma_w^2} \approx \frac{2\sqrt{2\pi} R_{wc}}{\gamma} \Delta S_o \tag{9}$$

where γ is a proportionality constant linking M_{12} and M_{21}. Hence, for near-neutral conditions, ejections and sweeps perturb gradient diffusion theory via an additive term given as

$$\overline{w'T'} = \underbrace{-\frac{\tau \sigma_w^2}{C_T} \frac{d\overline{T}}{dz}}_{\substack{Gradient-\\ Diffusion}} \underbrace{- \frac{\tau}{C_T} \frac{d}{dz} \left(\frac{2\sqrt{2\pi} \sigma_w^2 \sigma_T R_{wT}}{\gamma} \Delta S_o \right)}_{\substack{Perturbation\ to\ Gradient-Diffusion\\ due\ to\ ejections and sweeps}}. \tag{10}$$

While the analytical link in equation (10) is not prognostic, as the magnitude of ΔS_o is not a priori known, it is 'diagnostic' because it can offer some foresight as to how gradient-diffusion may fail for some regions or conditions based on what is already catalogued about the relative importance of ejections and sweeps in similar flows.

3. Experimental setup

The experiments were conducted during the 2009 growing season (i.e., May through October) in three hilly sites ideal for Nebbiolo and Barbera grapevines cultivars: (1) Cocconato (hereafter referred as CC: 45°05' N; 8°03' E; 311 m a.m.s.l.), (2) Fubine (hereafter FB: 44°58' N; 8°26' E; 210 m a.m.s.l.), and (3) Castiglione Falletto (hereafter CF: 44°37' N; 7°59' E; 275 m a.m.s.l.). In these sites, the vineyards were placed in rows 2.5 m apart from each other and trained on vertical shoot-positioned (VSP) systems, perpendicular to the contour lines (*rittochino*) at CC and aligned with them *(giropoggio*) at FB and CF. The orientation of the three slopes was south for CC, south-east for FB and east for CF. Fast response velocity and temperature measurements were sampled at 21 Hz using a 3-dimensional ultrasonic anemometer (Solent R2, Gill Instruments) installed at 3 m

above the soil surface (i.e., about one meter above the seasonal vegetation height peak). The interpretation of turbulent measurements is sensitive to the choice of the coordinate system. As a matter of fact, the 30-min mean wind component perpendicular to the surface ($\overline{w}$), unlike the mean horizontal one, is usually close to zero, implying that a small error in the *z*-axis positioning can introduce considerable inaccuracy in the measurement of *w*, thus invalidating the flux calculation. The coordinate system employed here is identified by the so-called planar fit method (Wilczak et al. 2001). The performance of this method and the data post-processing are presented in Appendix A for completeness. All time averages and mean quantities employed here are based on 30-minute periods. The local mean wind conditions during the experiment were generically low. The mode of the mean horizontal wind speed probability density function was around 0.7 m s^{-1}, regardless of the site. Not surprisingly, such low wind speed was often linked with small values of $\left|\overline{u'w'}\right|$. As earlier noted, ΔS_o becomes ill defined when $\left|\overline{u'w'}\right| \to 0$ and runs in which the friction velocity u_* was below 0.1 m s^{-1} were not considered. This filter removed 6,950 out 24,823 30-minute runs in the complete record at all three sites (for details see Table 1). In essence, when $\left|\overline{u'w'}\right|$ is so small, the study of ejection/sweep and updraft/downdraft contributions to momentum transfer become less important.

Table 1 also summarizes the main site characteristics and terrain slopes. Data are clustered according to changing LAI during the season in three subsets: begin season (i.e., LAI lower than 3 m^2m^{-2}), peak (i.e., LAI larger than 3 m^2m^{-2}), and end season (i.e., LAI again lower than 3 m^2m^{-2}). The threshold was chosen according to the typical seasonal vegetative trends of Nebbiolo and Barbera LAI in those sites (Francone et al., 2010) since the rapidly growing LAI tends to stabilize at the end of the growing season. Because canopy height is correlated with LAI, the latter was chosen as the primary variable describing the vegetation state.

4. Results and Discussion

The Results and Discussion section is structured so as to address three inter-related questions:

1) how do sloping terrain, LAI and thermal stratification jointly impact e_t and ΔS_o?
2) to what degree can the Gaussian JPDF and the CEM (and ICEM) describe e_t and ΔS_o for the range of sloping terrain, LAI, and thermal stratifications examined here?
3) to what extent can a variant on the MEH be employed to describe the flow statistics pertinent to e_t and ΔS_o as identified by the Gaussian JPDF (for e_t) and ICEM (for ΔS_o)?

The MEH was proposed by Kader and Yaglom (1978) for turbulent boundary layers subjected to adverse pressure gradients. These authors hypothesized that the free-stream velocity and the kinematic pressure gradient vary slowly with the horizontal coordinate, thereby retaining the local 'equilibrium state' between production and dissipation terms of the turbulent kinetic energy (TKE). Stated differently, the MEH assumes that in a boundary layer not too far from an equilibrium state, any position in the longitudinal direction depends on the relevant local flux-based boundary conditions and not on the upstream history of the flow. The implication of MEH to Question 3 is that the locally measured u_*, the sensible heat flux H_s, and the stability parameter $(z-d)/L$ may still be sufficient to describe the statistical moments needed for predicting e_t and ΔS_o via the approximations to the JPDF discussed in Question 2 (i.e., R_{ws}, M_{12}, and M_{21}). Here, z is the distance from the ground, d is the zero displacement level, and L is the Obukhov length.

4.1 Addressing Question (1)

In Table 1, the mean and the standard deviation of e_t and ΔS_o computed for both momentum and heat are listed for each site decomposed into the three vegetation periods, which in turn are further decomposed into two atmospheric stability conditions given by the stability parameter $(z-d)/L$. Among these control parameters, the terrain slope is notably less important after applying the planar fit method. LAI also has a minor effect on e_t and ΔS_o, whose mean (and standard deviation) values

remain comparable across the three vegetative periods. Thermal stratification appears the most relevant parameter for ΔS_o and e_t, especially for heat. Similar findings were presented in Bou-Zeid and Li (2011) for vineyards over flat surfaces. From the mean ΔS_o values reported in Table 1, it is evident that sweeps are major contributors to the momentum transfer for both stability cases. Also for heat transfer under stable (or nocturnal) stability conditions, sweeps dominate. Under unstable conditions, the heat transport is dominated by ejections. Similar results for momentum transfer near rough surfaces over flat and hilly terrain were already noted in a number of laboratory studies for momentum transfer and near-neutral conditions (e.g., Raupach, 1981; Poggi et al., 2007).

4.2 Addressing Question (2)

Question 2 is discussed in terms of the ability of the JPDF and CEM / ICEM approaches to describe measured e_t and ΔS_o, respectively, across all three sites, LAI variations, and stability classes. Figure 1 shows the comparison between measured and modeled e_t for FB as a reference, with model calculations conducted assuming a Gaussian JPDF (Equation 2). The modeled e_t describes well the observations regardless of sloping terrains, LAI values, and thermal stratification. In the case of heat transfer (Figure 1.b), the approach mildly underestimates mean absolute values of e_t in the upper part of the measured range, while standard deviation values fall along the 1:1 line. The same results were found for the other sites. It can be concluded that the correlation coefficient between w' and s' ($=u'$, T') or R_{ws} is an acceptable descriptor for capturing the main features of updraft/downdraft transport efficiency.

When this finding is taken jointly with the answer to Question 1, it motivates the exploration as to whether R_{uw} and R_{wT} can be described by the local atmospheric stability coefficient at each of the three sites. In Figure 2, the momentum and heat correlation coefficients are shown as a function of the atmospheric stability parameter, from the CC dataset as illustration. By and large, R_{uw} and R_{wT}

here fall close to expectations from flat-terrain atmospheric surface layer studies (Kaimal and Finnigan, 1994; Kader and Yaglom, 1990), with scatter generally not much larger than what was reported for flat terrain cases. Moreover, for the same atmospheric stability class, it is confirmed that the effects of variable leaf area index are not statistically significant. We have repeated this analysis for the other two sites with similar findings. These results suggest that sloping terrain and changing LAI are not significant discriminating factors for explaining variability in R_{uw}, R_{wT} when compared to atmospheric stability regime.

Table 2 shows the results of the linear regression between measured and modeled momentum and heat ΔS_o using CEM and ICEM for all three sites and only one LAI class chosen as representative. It is evident that both CEM and ICEM approaches reproduce well their quadrant analysis values (influenced by all the cumulants describing the JPDF). The coefficient of determination of both model fits lies between 0.86 and 0.97, and slopes and intercepts are respectively close to 1 and 0, respectively (comparison not shown). In particular, the slopes for ICEM are, in almost half of cases, more close to 1 than CEM ones, with all the remaining parameters being similar. The impact of varying slope and LAI on the momentum and heat ΔS_o was negligible for all three sites and stability conditions. It can be concluded that both approaches are equally suitable for the description of the relative importance of ejections and sweeps. It is worth noting that these results are in agreement with findings in Katul et al. (1997a) and Cava et al. (2006) for different forested canopies on flat terrain.

Given the good agreement between CEM, ICEM and quadrant analysis, as with the case of the e_t analysis, we then explored to what degree the statistical moments of the CEM (or a reduced version of them such as in the ICEM) can be predicted from local atmospheric stability conditions. As evidenced from Equations 4 to 7, the flow variables needed in the CEM/ICEM calculations of ΔS_o are R_{ws}, $M_{\alpha\beta}$, σ_w, and σ_s. The R_{ws} and its dependence on atmospheric stability conditions was already explored as part of the e_t analysis. In Raupach (1981), wind tunnel experiments over

various roughness configurations suggest that $M_{12} \approx -M_{21}$ for momentum irrespective of the surface roughness. Motivated by this finding, possible linear relationship between M_{12} and M_{21} was also explored for both heat and momentum, for all three sites, LAI and stability classes. Table 3 reports the slope and intercept obtained from linear regression for momentum and heat among the triple moments for the three sites, and Figure 3 shows M_{21} as a function of M_{12} at the CC site, as illustrative. Indeed, these dimensionless mixed moments are linearly related and this relationship is not significantly dependent on terrain slope. Varying LAI impacted the linear regression slope, especially during the period when LAI was transitioning from its minimum to its peak and under unstable conditions, for both momentum and heat. The atmospheric stability parameter was less relevant in explaining any shift in the linear relationships for momentum. Nevertheless, as with the transport efficiency and quadrant analysis, the stability parameter was the main influencing factor characterizing the linear relationship between heat M_{21} and M_{12}. In particular, differences in slope and also intercept values where found with a change in slope sign occurring with stability class independent from LAI and site slope. Table 3 suggests that $0.3 \le \left|M_{21}/M_{12}\right| \le 0.6$ for momentum and heat and for unstable and stable conditions. These results are comparable with Cava et al. (2006) who reported $\left|M_{21}/M_{12}\right| \approx 0.6$ for momentum and heat transfer under different atmospheric stability classes above a dense forest.

In Figure 4, a relationship between M_{21} and the atmospheric stability parameter was also explored at one site (CC), again used here as a case study. The CC data suggest that the M_{21} for momentum was slightly dependent on varying LAI, especially under unstable condition, while it was invariant to atmospheric stability class. In the case of heat, M_{21} varied with atmospheric stability only under unstable conditions, while different LAI values remained comparable within the scatter. This analysis was repeated for the other two sites and it demonstrated that different terrain slopes did not significantly impact the relations found here.

Finally, Figure 5 shows the variations in σ_w, σ_u and σ_T with atmospheric stability along with the dimensionless similarity functions reported for flat surfaces (Kaimal and Finnigan, 1994; Kader and Yaglom, 1990; Cava et al., 2008). The outcome of this analysis is that analogous to R_{ws}, the normalized velocity variances closely following their counterparts for flat-terrain conditions. For temperature, the scatter is significantly larger when compared to velocity, especially for near-neutral and mildly stable runs (Figure 5.f). Under those conditions, it is known that $T_* = -\overline{w'T'}/u_*$ is small, and hence, σ_T / T_* becomes sensitive to instrument noise and any other source of non-stationarity that contaminates σ_T but not $\overline{w'T'}$. Hence, it is expected that σ_T / T_* takes on large values under those conditions as supported by the scatter in Figure 5.

4.3 Addressing Question (3)

In analyzing the applicability of MEH to such a setup, it may be helpful to note that, in a first order analysis, the mean pressure gradients are produced by the topographic variability. These pressure gradients are then responsible for the generation of advective acceleration terms, which in turn disturb the mean flow gradients. The turbulent fluxes adjust to these disturbed mean flow gradients, thereby introducing turbulent flux gradient terms at a given point. At the three sites studied, and when employing the planar fit method at a point, the mean lateral and vertical velocities are forced to be zero. Hence, the effects of all the advective terms are encoded in the mean longitudinal advection. As mentioned earlier, the mean horizontal wind speed issmall at all sites, hinting that large advective terms do not occur frequently. These results, together with the outcome of Figures 2 and 5, do support the use of MEH for R_{ws}, σ_w and σ_T in that local atmospheric stability conditions describe their main variations as was the case for flow over flat surface. As a matter of fact, Figure 2 suggests that MEH can be used to predict the relative efficiencies of updrafts and downdrafts (R_{ws} is the main variable describing e_t). Figure 5 also shows the normalized velocity and temperature

standard deviations as a function of atmospheric stability conditions follow their flat-terrain counterpart. These results strengthen the application of MEH to such types of tilted terrain and inhomogeneous canopy, with the effects of the advective terms and mean pressure gradients partly absorbed by the planar fit coordinate system. Moreover, when this finding is taken jointly with the ICEM predictive skills and the analysis of M_{12} and M_{21} in Figure 4 and Table 3, it appears that ΔS_o can also be explained by MEH, thereby addressing Question 3.

5. Conclusions

Three inter-related questions about the properties of ejections/sweeps and updraft/downdrafts were explored at three sites with different terrain slopes experiencing a wide range of variations in leaf area density and in thermal stratification conditions. The analysis was performed after the employment of the planar fit method to transform the wind velocity components in a coordinate system with the *z*-axis perpendicular to the terrain. With regards to the first question (how do sloping terrain, LAI, and thermal stratification jointly impact e_t and ΔS_o), it was shown that thermal stratification plays the primary role. It was also shown that, under unstable conditions, sweeping motion dominates momentum transport at fractional contributions commensurate with canopy studies over flat terrain. For heat, ejections dominate for unstable conditions while sweeps dominate for stable conditions, as is the case for flat terrain. With regards to the second question (to what degree can the Gaussian JPDF, the CEM, and the ICEM describe e_t and ΔS_o), it was shown that the agreement between measurements and predictions was reasonable for all three sites, thermal stratification, and leaf area index. Finally, with regards to the third question (to what extend can the MEH describe the flow statistics pertinent to e_t and ΔS_o), it was shown that these statistics can be described by the local atmospheric stability parameter at all sites and for all leaf area values, again showing relationships comparable to those reported for flat terrain cases. The notable exception was the relationship between M_{12} and M_{21}, which diverged from its expected behavior as derived from

wind-tunnel studies for momentum ($M_{12} \approx -M_{21}$). However, the linearity between M_{12} and M_{21}, for heat and momentum, was maintained with a regression slope that varies primarily with atmospheric stability and secondarily with leaf area.

Given the good performance of the ICEM and the linearity between M_{12} and M_{21} across a wide range of slopes, LAI, and stability classes noted here, equation (10) does offer some foresight as to when and why gradient-diffusion approximation may fail, at least where the relative importance of ejections and sweeps in similar flows is a priori catalogued. This linkage between ejections and sweeps and corrections to gradient-diffusion theories is a logical step to progress on practical problems such as those pertinent to regulating heat accumulation, modeling inversion layers at near-freezing conditions, and modeling of dry air entrainment from above the canopy in case of fungicide diseases.

Appendix A - Planar fit method and data post processing

The Planar Fit Method (PFM hereinafter) was proposed by Wilczak et al. (2001) to minimize the anemometer positioning error when turbulent fluxes are computed. It is based on the premise that if the mean flow, independently from its direction, occurs in a plane, this plane can be determined from the analysis of a long series of wind measurements by taking a two-dimensional linear regression of the velocity component perpendicular to the plane versus the parallel ones. In the present work, the PFM was applied to datasets from each station and the flow planarity, as well as the orientation of the flow planes, have been evaluated as detailed in Richiardone et al. (2008). Pre-processing of data involved correction for the misalignment between the assembly of the sonic transducers and the anemometer pedestal. The velocity of the plane vectors have been handled following the physics convention: contrarily to the common meteorological convention, their directions indicate the direction towards which the wind blows (i.e., 90° for a westerly wind). Figure A1 shows, for each station, the tilt above the horizontal of each 10°-wide sector mean velocity vector versus the sector direction (points with error bars in Fig. A1). If the velocity vectors are positioned exactly on the PFM planes, their tilt above the horizontal would vary sinusoidally with their azimuthal direction (continuous lines in Fig. A1) . Their tilt would reach the maximum value v_{PFM} at direction ω_{PFM} (Table A1), and would become null at right angles, where the vectors would become parallel to the horizontal plane. Incidental and systematic deviations of the velocity vector tilt from the sinusoid indicate a flow distortion with respect to the plane. Fig. A1 shows that the agreement between the mean velocity tilt and the PFM plane tilt curves is acceptable in all stations, with some distortion at CF and (very small) at FB. At all stations, the mean flow can be considered planar, with about the same 10° tilt and a similar orientation at CC and FB (south and south-east, respectively). CF is the steepest place (17° tilt) and is east-oriented. The values of the plane surface tilt along the west-east (θ_{PFM}) and south-north (φ_{PFM}) directions have been derived from the PFM estimate of the plane orientation, and are compared with their measured values in Table A1. In spite of the local ground inhomogeneities, the agreement between PFM estimate and

measurements is quite good. Therefore, PFM is a convenient method when evaluating the planarity of the mean flow and the direction normal to the ground surface, i.e., to determine the z-axis of the coordinate systems to be used in turbulence studies. The x-axis is usually chosen aligned along the horizontal component of the mean velocity vector. In the present study, the actual (x, y, z) coordinate system used in the evaluation of the turbulent variables has been re-defined every 30 minutes by means of a rotation around the z-axis (constant throughout the experimental period) to maintain the x-axis aligned with the 30-min mean wind direction.

Acknowledgements

C. Francone, R. Richiardone and C. Cassardo acknowledge the financial support from the Regione Piemonte (Italy) under the MASGRAPE – CIPE 2006 project titled "Adoption of a multisciplinary approach to study the grapevine agroecosystem: analysis of biotic and abiotic factors able to influence yield and quality". G. Katul acknowledges the financial support from the U.S. Department of Energy through the Office of Biological and Environmental Research (BER) Terrestrial Ecosystem Science (TES) Program (DE-SC0006967), the U.S. National Science Foundation (NSF-AGS-1102227, NSF-CBET 103347, NSF-EAR-10-13339), the U.S. Department of Agriculture (2011-67003-30222), and the Fulbright-Italy distinguished scholars program. Part of this work was initiated during a Summer School on "Biogeodynamics and Earth System Sciences" organized by the Istituto Veneto di Scienze Lettere ed Arti (Venice, June 11-18 2010).

References

Antonia, R.A., 1981. Conditional sampling in turbulence measurements. Annu. Rev. Fluid Mech. 13, 131-156.

Bou-Zeid, E., Li, D., 2011. Coherent structures and the dissimilarity of turbulent transport of momentum and scalars in the unstable atmospheric surface layer. Bound. Layer. Meteorol. DOI: 10.1007/s10546-011-9613-5.

Cantwell, B.J., 1981. Organized motion in turbulent flow. Ann. Rev. Fluid Mech. 13, 457-515.

Cava, D., Katul, G.G., Scrimieri, A., Poggi, D., Cescatti, A., Giostra, U., 2006. Buoyancy and the sensible heat flux budget within dense canopies. Boundary-Layer. Meteorol. 118, 217-240.

Cava, D., Katul, G.G., Sempreviva, A.M., Giostra, U., Scrimieri, A., 2008. On the anomalous behaviour of scalar flux-variance similarity functions within the canopy sub-layer of a dense alpine forest, Bound. Layer Meteorol. 128, 33-57.

Finnigan, J.J., 2000. Turbulence in plant canopies. Annu. Rev. Fluid Mech. 32, 519-571.

Finnigan, J.J. and Belcher, S.E., 2004. Flow over hill covered with a plant canopy, Quart. J. Roy. Meteorol. Soc. 130 (596), 1-29.

Francone, C., Cassardo, C., Spanna, F., Alemanno, L., Bertoni, D., Richiardone, R., Vercellino, I., 2010. Preliminary results on the evaluation of factors influencing evapotranspiration processes in vineyards. Water, 2, 916-937.

Gao, W., Shaw, R.H., Paw U.K.T., 1989. Observation of organized structure in turbulent flow within and above a forest canopy. Bound. Layer Meteorol. 47, 349-377.

Garratt JR (1992) The atmospheric boundary layer. Cambridge University Press, UK, p. 316.

Hicks, B.B., 1973. Eddy fluxes over vineyards. Agric. Meteorol. 12, 203-215.

Kader, B.A., Yaglom, A.M., 1978. Similarity treatment of moving-equilibrium turbulent boundary layers in adverse pressure-gradients. J. Fluid Mech. 89, 305-342.

Kader, B.A. and Yaglom, A.M., 1990. Mean fields and fluctuation moments in unstably stratified turbulent boundary layers. J. Fluid Mech. 212, 637-662.

Kaimal, J.C., Finnigan, J.J., 1994. Atmospheric Boundary Layer Flows: Their Structure and Measurement, Oxford University Press, New York, p. 289.

Kampé de Fériet, J., 1966. The Gram-Charlier approximation of the normal law and the statistical description of a homogeneous turbulent flow near statistical equilibrium. Model Basin Report No. 2013, Naval Ship Research and Development Center, Washington, DC.

Katul, G.G., Hsieh, C.I., Kuhn, G., Ellsworth, D., Nie, D., 1997a. The turbulent eddy motion at the forest-atmosphere interface. J. Geophys. Res. 102, 13409-13421.

Katul, G.G., Kuhn, G., Scheildge, J., Hsieh, C.I., 1997b. The ejection-sweep character of scalar fluxes in the unstable surface layer, Bound. Layer Meteorol., 83, 1-26.

Katul, G.G., Poggi, D., Cava, D., Finnigan, J., 2006. The relative importance of ejections and sweeps to momentum transfer in the atmospheric boundary layer, Bound. Layer Meteorol., 83, 1-26.

Kline, S.J., Reynolds, W.C., Schraub, F.A., Runstadler, P.W., 1967. The structure of turbulent boundary layers. J. Fluid Mech. 30, 741-773.

Lu, S.S., Willmarth, W.W., 1973. Measurements of the structure of Reynolds stress in a turbulent boundary layer. J. Fluid Mech. 60, 481-571.

Nakagawa, H., Nezu, I., 1977. Prediction of the contributions to the Reynolds stress from bursting events in open channel flows. J. Fluid Mech. 80, 99-128.

Poggi, D., Katul, G.G., Albertson, J.D., 2004. Momentum transfer and turbulent kinetic energy budgets within a dense model canopy. Bound. Layer Meteorol. 111, 589−614.

Poggi, D., Katul, G.G., 2007. The ejection-sweep cycle over gentle hills covered with bare and forested surfaces. Boundary Layer Meteor. 122, 493-515.

Poggi, D., Katul, G.G., Finnigan, J.J., Belcher, S.E., 2008. Analytical models for the mean flow inside dense canopies on gentle hilly terrain. Quart. J. Roy. Meteorol. Soc. 134, 1095-1112.

Raupach, M.R., Thom, A.S., 1981. Turbulence in and above plant canopies. Ann. Rev. Fluid Mech. 13, 97-129.

Raupach, M.R., 1981. Conditional statistics of Reynolds stress in rough-wall and smooth-wall turbulent boundary layers. J. Fluid Mech. 108, 363-382.

Raupach, M.R., Weng, W.S., Carruthers, D.J., and Hunt, J.C.R., 1992. Temperature and humidity fields and fluxes over low hills. Quart. J. Roy. Meteorol. Soc. 118, 191-225.

Raupach, M.R., Finnigan, J.J., Brunet, Y., 1996. Coherent eddies and turbulence in vegetation canopies: the mixing layer analogy. Bound. Layer Meteorol. 78, 351-382.

Raupach, M.R. and Finnigan, J.J., 1997. The influence of topography on meteorological variables and surface-atmosphere interactions. J. Hydrol. 190, 182-213.

Riou, C., Pieri, P. and Volancogne, C., 1987. Variation de la vitesse du vent a l'interieur et au-dessus d'une vigne. Agric. For. Meteorol. 39, 143-154.

Richiardone, R., Giampiccolo, E., Ferrarese, S., Manfrin, M., 2008. Detection of flow distortions and systematic errors in sonic anemometry using the planar fit method, Bound. Layer Meteorol. 128, 277-302.

Robinson, S.K., 1991. Coherent motions in turbulent boundary layers. Annu. Rev. Fluid Mech. 23, 601-639.

Shaw, R.H., Tavangar, J., Ward, D., 1983. Structure of the Reynolds stress in a canopy layer. J. Clim. Appl. Meteor. 22, 1922-1931.

Weiss, A., Allen, L.H., 1976. Vertical and horizontal air flow above rows of a vineyard. Agric. Meteorol. 17, 433-452.

Wilczak, J.M., Oncley, S.P., Stage, S.A., 2001. Sonic anemometer tilt correction algorithms. Bound. Layer Meteorol. 99, 127-150.

Wilson, J.D., Finnigan, J.J., Raupach, M.R., 1998. A first order closure for disturbed plant-canopy flows and its application to winds in a canopy on a ridge. Quart. J. Roy. Meteorol. Soc. 124, 705-732.

Wyngaard, J.C., Moeng, C.-H., 1992. Parameterizing turbulent diffusion through the joint probability density. Bound. Layer Meteor. 60, 1-13.

Tables

Table 1. The main features of the datasets at the three sites grouped according to the vegetative cycle and atmospheric stability conditions. The terms - *begin season* (i.e., LAI < 3 $m^2 m^{-2}$,dLAI/dt > 0), *peak* (i.e., LAI > 3 $m^2 m^{-2}$) and *end season* (i.e., LAI < 3 $m^2 m^{-2}$, dLAI/dt < 0) - are used to classify the vegetative state, where t is time. The maximum canopy height for each of these vegetative cycles is shown. Throughout, a positive slope indicates an upward tilt (e.g., N higher than S in S-N direction). The fraction of runs in which $u_* > 0.1$ m s^{-1} is also presented. The ensemble-averaged e_t and ΔS_o along with their standard deviations are also shown for each stability class.

site	***slope (W-E dir.)***	***slope (S-N dir.)***	***canopy height***	***$u_* > 0.1$***	***stability conditions***	***MOMENTUM***		***HEAT***	
	(°)	(°)	(m)	(% events)		e_t	ΔS_0	e_t	ΔS_0
						mean ± std	***mean ± std***	***mean ± std***	***mean ± std***
CC	−2.7	8.9							
Begin season			1.4	57.4	*Stable*	0.49±0.15	0.32±0.21	0.53±0.18	0.03±0.30
					Unstable	0.36±0.18	0.19±0.26	0.77±0.14	−0.19±0.11
Peak			1.9	71.5	*Stable*	0.53±0.15	0.37±0.25	0.55±0.17	0.13±0.26
					Unstable	0.49±0.15	0.29±0.20	0.74±0.15	−0.13±0.16
End season			1.8	57.8	*Stable*	0.54±0.15	0.36±0.25	0.54±0.17	0.14±0.28
					Unstable	0.52±0.15	0.26±0.21	0.76±0.16	−0.13±0.16
FB	−7.2	5.8							
Begin season			1.5	57.4	*Stable*	0.47±0.18	0.23±0.20	0.50±0.20	0.13±0.23
					Unstable	0.45±0.19	0.12±0.31	0.69±0.21	−0.15±0.18
Peak			2.4	71.5	*Stable*	0.62±0.13	0.35±0.25	0.57±0.15	0.12±0.26
					Unstable	0.54±0.16	0.28±0.27	0.75±0.14	−0.11±0.15
End season			2.2	57.8	*Stable*	0.64±0.14	0.33±0.25	0.57±0.17	0.13±0.28
					Unstable	0.59±0.16	0.31±0.25	0.75±0.17	−0.06±0.19
CF	−17.6	−7.2							
Begin season			1.2	86.8	*Stable*	0.66±0.15	0.18±0.33	0.58±0.18	0.08±0.32
					Unstable	0.36±0.20	0.11±0.30	0.71±0.17	−0.15±0.23
Peak			2.2	66.8	*Stable*	0.58±0.17	0.29±0.22	0.55±0.18	0.17±0.27
					Unstable	0.41±0.19	0.28±0.20	0.74±0.17	−0.15±0.18
End season			1.9	77.6	*Stable*	0.60±0.17	0.28±0.21	0.54±0.19	0.21±0.29
					Unstable	0.47±0.18	0.25±0.18	0.73±0.19	−0.14±0.20

Table 2. Linear regression analysis (i.e. $y = ax + b$) with $y = \Delta S_0$ modeled using CEM and ICEM approaches against $x = \Delta S_0$ directly estimated via quadrant analysis for the three sites and end season vegetative state. The r^2 here is the coefficient of determination.

Site	***Stability conditions***	***MOMENTUM***			***HEAT***		
		a	***b***	***r²***	***a***	***b***	***r²***
CC							
CEM	*Stable*	1.03	0.00	0.95	1.07	0.00	0.88
	Unstable	0.96	0.01	0.92	0.93	0.01	0.97
ICEM	*Stable*	1.09	0.02	0.93	0.99	0.02	0.91
	Unstable	0.98	0.03	0.90	0.99	−0.02	0.94
FB							
CEM	*Stable*	0.97	0.01	0.96	0.94	0.01	0.97
	Unstable	1.00	0.00	0.94	0.90	0.01	0.96
ICEM	*Stable*	1.08	0.02	0.92	0.95	0.02	0.95
	Unstable	1.08	0.02	0.92	0.95	−0.01	0.94
CF							
CEM	*Stable*	0.99	0.00	0.90	0.95	0.01	0.96
	Unstable	0.99	−0.01	0.87	0.95	0.01	0.93
ICEM	*Stable*	1.04	0.03	0.88	0.92	0.02	0.94
	Unstable	1.03	0.01	0.86	1.04	−0.01	0.93

Table 3. Linear regression analysis (i.e. $y = ax + b$) with $y = M_{21} = \overline{s'w'w'}/(\sigma_s^2 \sigma_w)$ against $x = M_{12} = \overline{s'w'w'}/(\sigma_s \sigma_w^2)$ for the three sites.

site	***stability conditions***	***s'=u' (MOMENTUM)***		***s'=T' (HEAT)***	
		a	***b***	***a***	***b***
CC					
Begin season	*Stable*	−0.40	−0.02	−0.39	0.07
	Unstable	−0.20	−0.04	0.61	0.18
Peak	*Stable*	−0.36	−0.07	−0.22	0.03
	Unstable	−0.37	−0.10	0.42	0.19
End season	*Stable*	−0.45	−0.05	−0.23	0.01
	Unstable	−0.43	−0.08	0.49	0.16
FB					
Begin season	*Stable*	−0.31	−0.04	−0.28	0.02
	Unstable	−0.31	−0.05	0.71	0.15
Peak	*Stable*	−0.52	−0.02	−0.31	0.02
	Unstable	−0.46	−0.08	0.53	0.18
End season	*Stable*	−0.53	−0.04	−0.30	0.01
	Unstable	−0.48	−0.08	0.56	0.16
CF					
Begin season	*Stable*	−0.58	−0.03	−0.30	0.04
	Unstable	−0.24	−0.04	0.70	0.11
Peak	*Stable*	−0.47	−0.05	−0.28	0.05
	Unstable	−0.29	−0.09	0.57	0.20
End season	*Stable*	−0.47	−0.06	−0.35	0.04
	Unstable	−0.33	−0.10	0.66	0.15

Table A1. Plane tilt maximum value (ν_{PFM}) and relative direction (ω_{PFM}, clockwise from north) calculated by the planar fit. Comparison of the PFM plane surface tilt along the west-east (θ_{PFM}) and south-north (φ_{PFM}) directions against their measured values (θ_{meas}, φ_{meas}). Positive values indicate an upward tilt.

	$\nu_{PFM}\pm\sigma$ (°)	$\omega_{PFM}\pm\sigma$ (°)	$\theta_{PFM}\pm\sigma$ (°)	θ_{meas} (°)	$\varphi_{PFM}\pm\sigma$ (°)	φ_{meas} (°)
CC	9.4	351	−1.4	−2.7	9.3	8.9
FB	10.4	315	−7.3	−7.2	7.4	5.8
CF	16.9	257	−16.5	−17.6	−3.9	−7.2

Figures

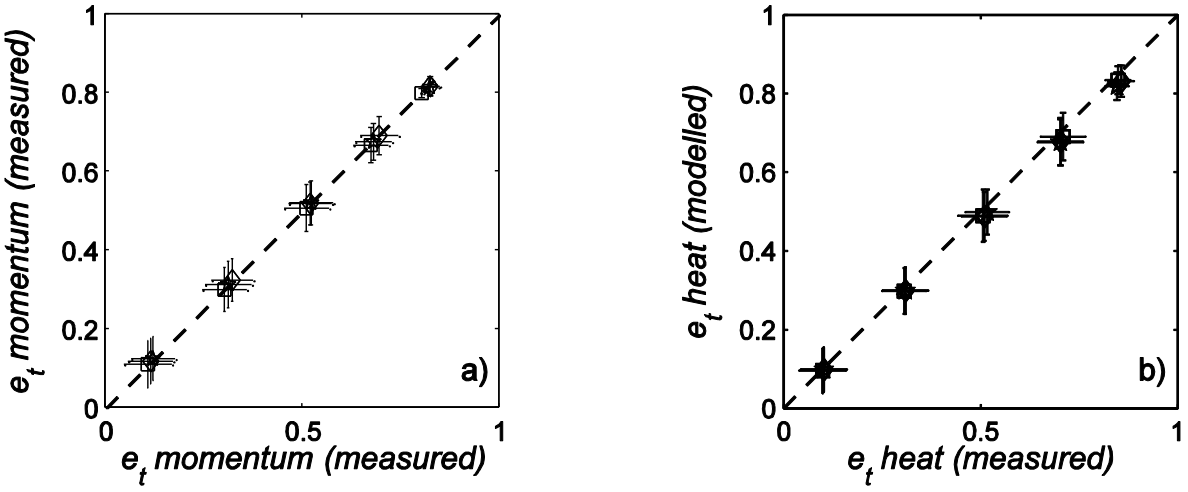

Figure 1. Comparison between measured and modeled transport efficiency (e_t) for momentum (a) and heat (b) at the FB site. The modeled e_t is calculated from a Gaussian JPDF. Data are grouped according to the vegetative cycle. Beginning season LAI (squares), peak LAI (diamond) and end season LAI (stars). Data are clustered in 0.2-wide bins of measured e_t and each point represents the mean values and error bars the standard deviations of both axis variables. 1:1 line is shown for reference.

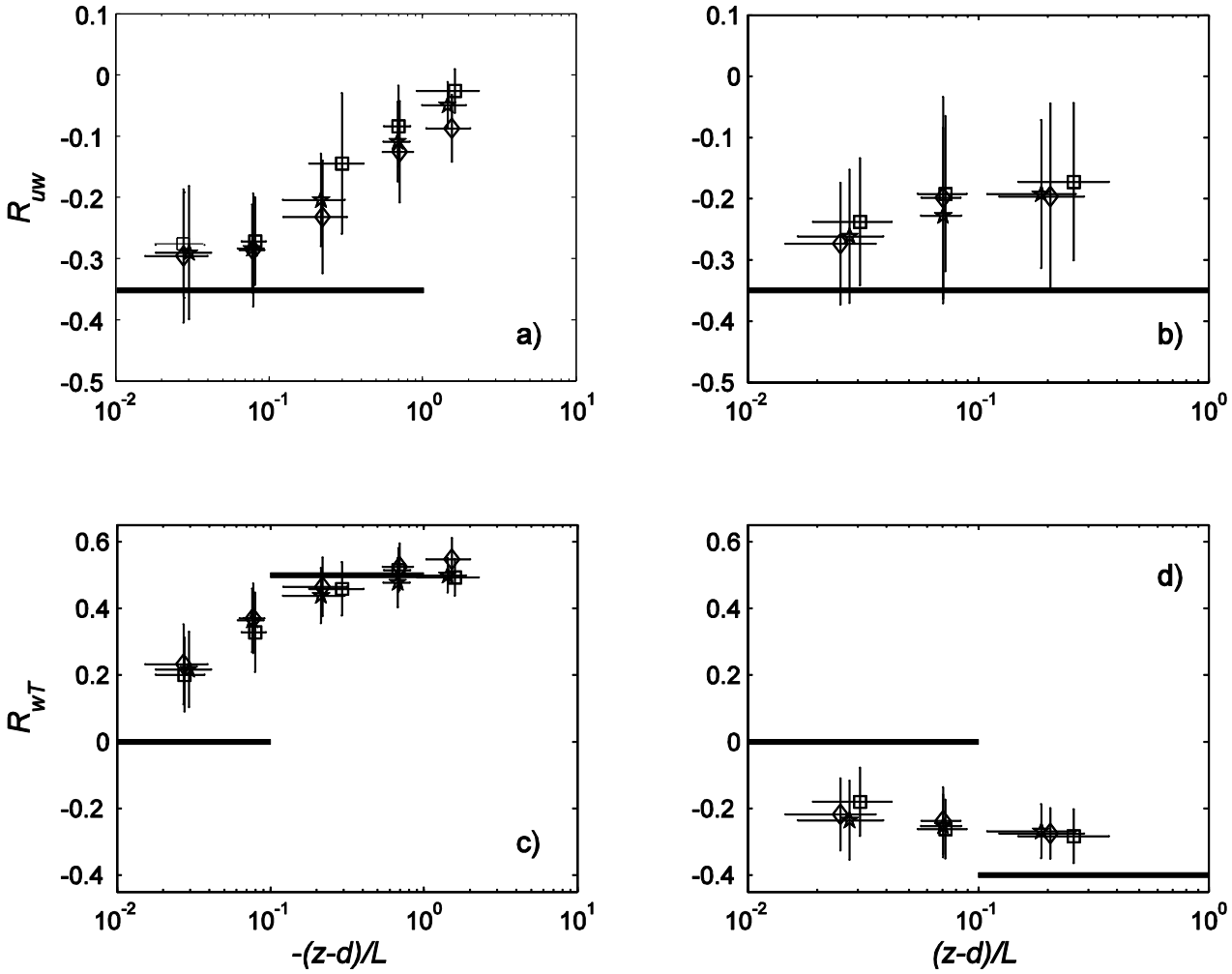

Figure 2. The correlation coefficient for momentum R_{uw} (a, b) and heat R_{wT} (c, d) as a function of the atmospheric stability parameter (unstable conditions: left column, and stable conditions: right column) for CC (mild slope) site. Data are grouped according to the vegetative cycle with symbols defined as in Figure 1. Data are clustered in half-order-of-magnitude-wide bins of stability coefficient, since horizontal axes scale is logarithmic. Each point represents the mean values and error bars are the standard deviations of both axis variables. Relationships reported for flat terrain are also shown (thick lines from Kaimal and Finnigan, 1994).

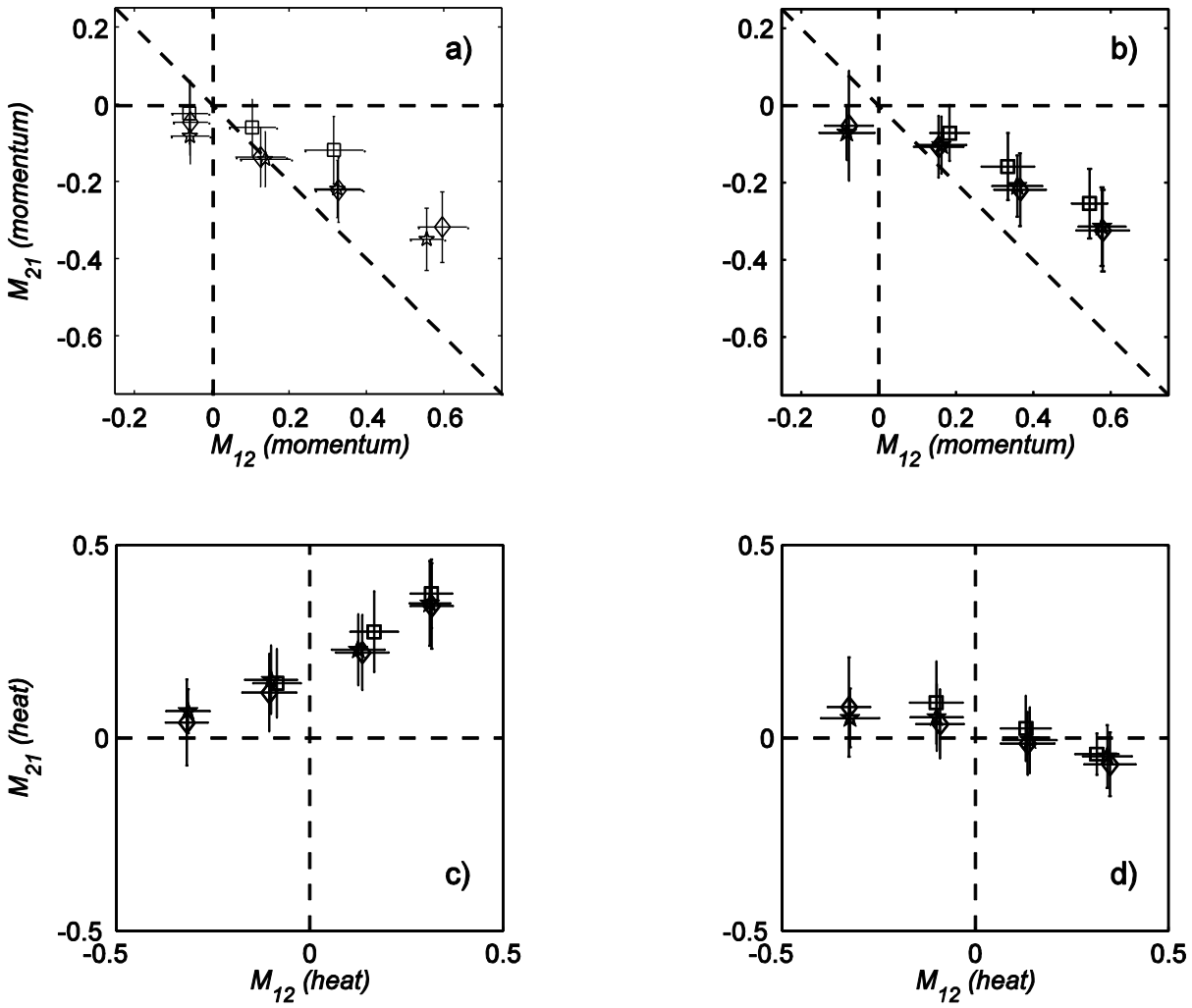

Figure 3. Mixed moment M_{21} as a function of M_{12} for momentum (a, b) and for heat (c, d) from the CC site. Left (right) column shows the comparisons under unstable (stable) conditions. Symbols are defined as in Figure 1. Data are clustered in 0.25-wide bins of M_{21}. Each point represents the mean value and error bars are the standard deviations of both axis variables. In panels (a) and (b), the linear relationship derived from wind tunnel studies by Raupach (1981) is also shown.

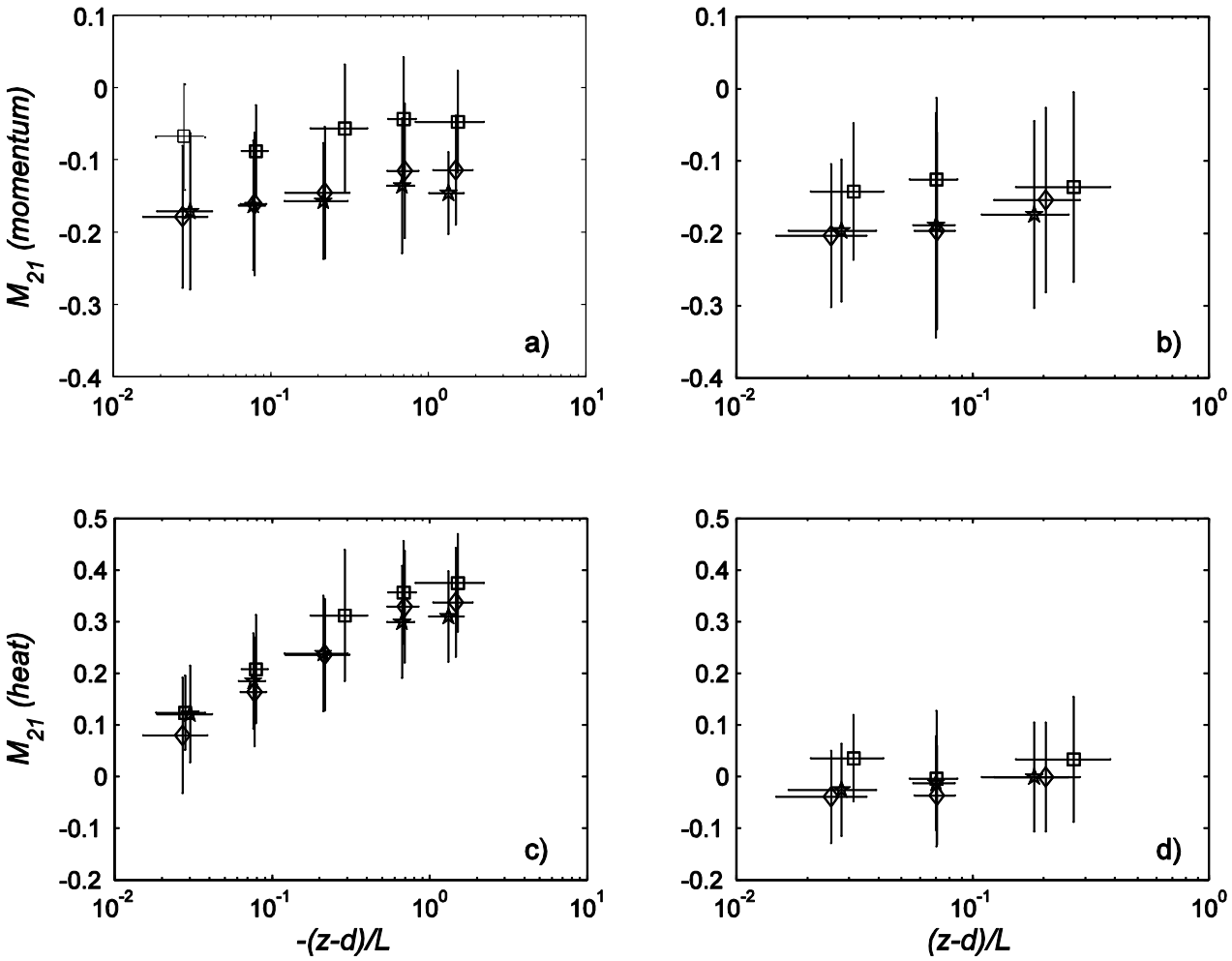

Figure 4. Mixed moment M_{21} as a function of the stability coefficient for momentum (a, b) and for heat (c, d) from the CC site. Left (right) column reports data under unstable (stable) conditions. Symbols are defined as in Figure 1. Data are clustered in half-order-of-magnitude-wide bins of stability coefficient, since the horizontal axis scale is logarithmic. Each point represents the mean value and error bars are the standard deviations of both axis variables.

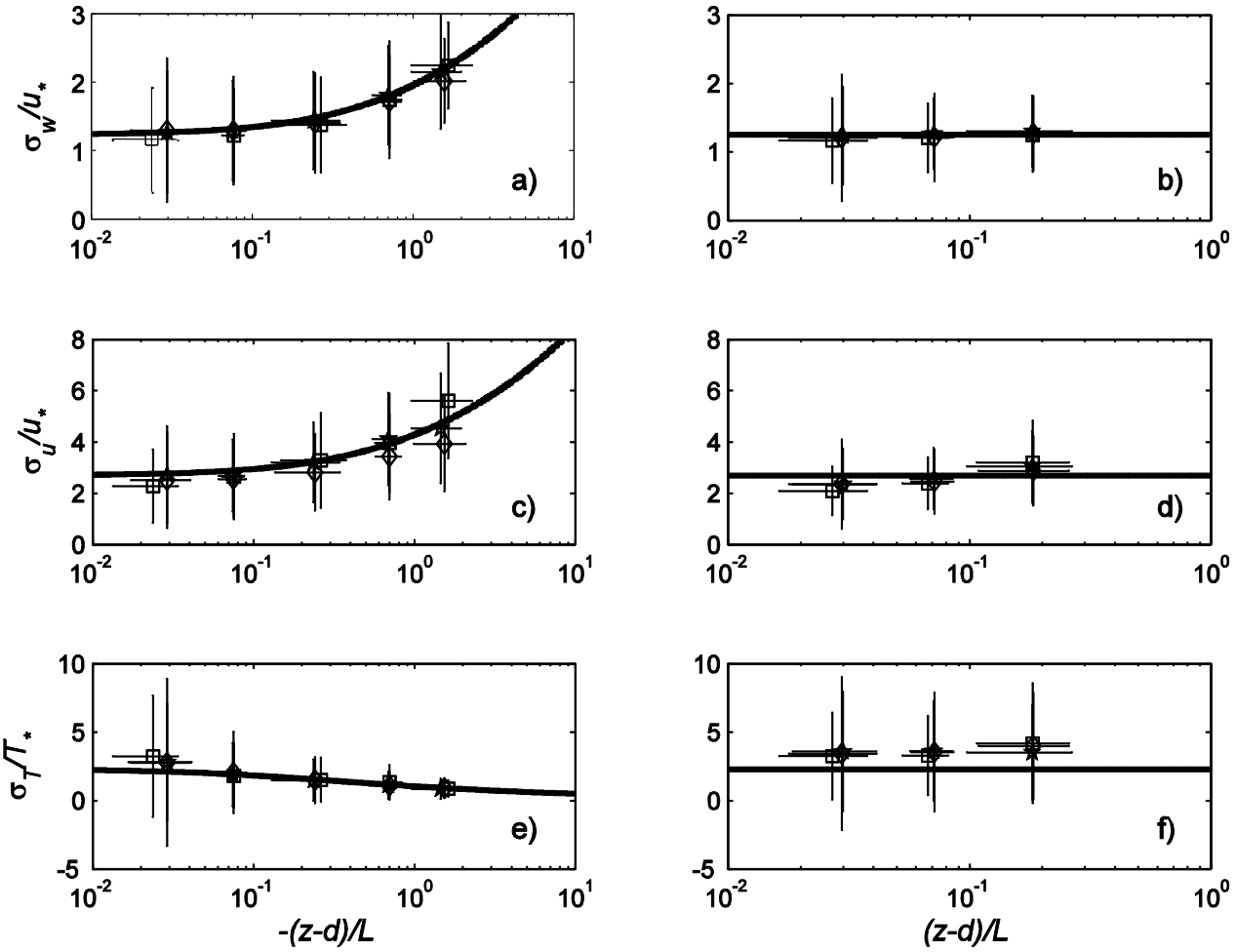

Figure 5. Longitudinal (a, b), vertical (c, d) velocity and temperature (e, f) standard deviations for unstable conditions (left column) and stable conditions (right column) from the steepest site (CF). Normalizing parameters are: $u_* = \left(\overline{v'w'}^2 + \overline{u'w'}^2\right)^{\frac{1}{4}}$ and $T_* = \frac{\overline{w'T'}}{u_*}$. Symbols are defined as in Figure 1. Relations superimposed (thin lines) are from Kader and Yaglom (1990) (a, b, c, d) and from Cava et al. (2008) (e, f). Data are clustered in half-order-of-magnitude-bins, since the horizontal axis scale is logarithmic. Each point represents the mean value and error bars are the standard deviations of both axis variables.

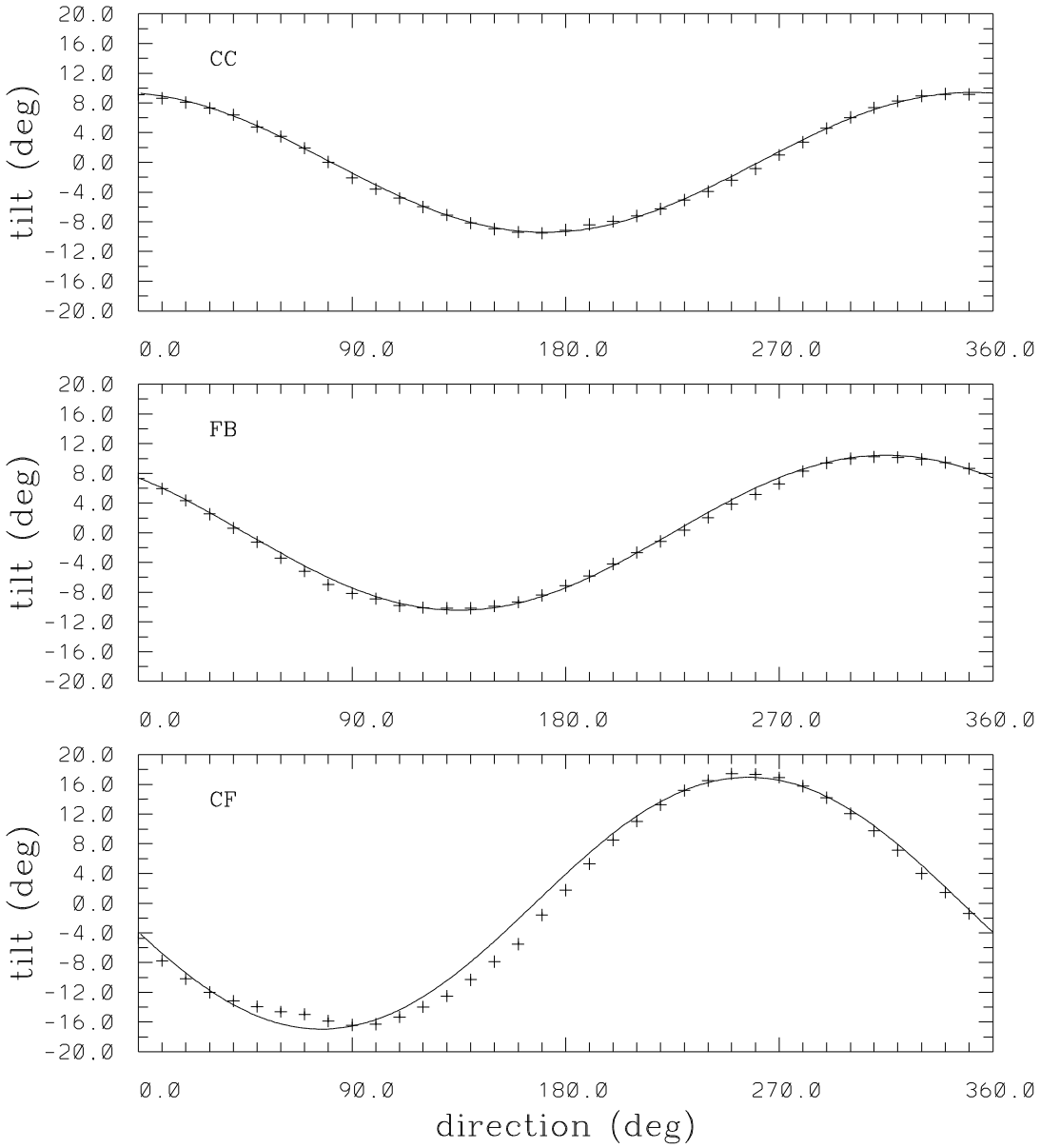

Figure A1. Azimuthal distribution of the 10°-wide-sector mean velocity vector tilt above the horizontal plane at CC (top), FB (middle) and CF (bottom) stations. The continuous curves indicate the predicted values if the velocity vectors lie exactly on the PFM plane. The velocity vector direction (clockwise from north) indicates the direction towards which the wind blows.